Available online at www.sciencedirect.com
SCIENCE DIRECT®
PERGAMON
Applied Geochemistry 18 (2003) 1081–1093
Applied Geochemistry
www.elsevier.com/locate/apgeochem

Potential for travertine formation: Fossil Creek, Arizona

John Malusa[a], Steven T. Overby[b,*], Roderic A. Parnell[a]

[a]*Department of Geology, Northern Arizona University, Flagstaff, AZ 86001, USA*
[b]*Rocky Mountain Research Station, USFS, 2500 S. Pine Knoll, Flagstaff, AZ 86001, USA*

Received 2 April 2002; accepted 18 October 2002
Editorial handling by R. L. Bassett

Abstract

Chemical analyses of water emanating from Fossil Springs in Central Arizona were conducted to predict changes in travertine deposition related to changes in stream discharge caused by diversion for hydroelectric power generation. During spring of 1996, water was sampled at 15 locations during normal seepage flow in a 6.7 km reach below Fossil Springs and at full baseflow during turbine maintenance. Analyses resulted in a rate of 11,923 kg d^{-1} of $CaCO_3$ precipitated from 1218 l s^{-1} of water emanating from the springs, while flows of 5.6 l s^{-1} that seep past a diversion dam produced 46 kg d^{-1} of $CaCO_3$ precipitation. Active travertine dams currently occur predominantly below the Irving hydroelectric powerplant with partial return of diverted flow back into the natural channel. The lower reach resulted in 519 kg d^{-1} of $CaCO_3$ precipitated from the return of 56.6 l s^{-1} with a reduced rate of precipitation during surface runoff conditions due to a dilution effect. Artificial substrates were located at sites in the lower reach for comparison with mass transfer rates derived from changes in water chemistry. Comparison between actual precipitation rates and overall mass transfer rates suggested preferential deposition was occurring at dam locations. Rates of mass transfer for high flow were greater than lower flow. Overall, mass transfer rates for the upper reach were proportional to the flow velocities with total mass transfers for both flows being approximately equal.

1. Introduction

Springs emitting supersaturated water with respect to $CaCO_3$ have the potential to create travertine structures that dramatically alter stream morphology. These structures are formed by an unusual combination of natural processes. Notable examples of these geomorphic structures include Mammoth Hot Springs in Yellowstone National Park, Montana, USA; Huanglong Natural Scenic District in Sichuan, China; Cascadas de Agua Azul, Chiapas, Mexico; and Havasu Creek, Supai Reservation, Arizona, USA.

Formation begins when water interacts with the soil zone, carbonate aquifers, organic material, or regional geothermal activity to produce H_2CO_3 (Stumm and Morgan, 1981; Pentecost, 1995; Deines, 1992; Cathelineau et al., 1989; Barnes et al., 1984; Hurley et al., 1966, Friedman, 1970). The H_2CO_3 increases dissolution of carbonate rocks resulting in elevated dissolved CO_2 concentrations in the water. The concentration gradient between atmospheric CO_2 and dissolved CO_2 in water emerging from an aquifer initiates outgassing (Jacobson and Langmuir, 1970; Langmuir, 1971). As CO_2 concentrations move toward equilibrium through outgassing, the water becomes supersaturated with $CaCO_3$, eventually reaching a critical level. When this critical level is exceeded, a kinetic barrier is surpassed and $CaCO_3$ precipitates to form travertine deposits (Stumm and Morgan, 1981; Dandurand et al., 1982).

Located in central Arizona (Fig. 1), Fossil Springs provides an opportunity for studying precipitation dynamics of a travertine-depositing spring. Within

* Corresponding author.
E-mail address: soverby@fs.fed.us (S. T. Overby).

0883-2927/03/$ - see front matter © 2003 Elsevier Science Ltd. All rights reserved.
doi:10.1016/S0883-2927(02)00241-X

Fossil Creek Canyon, numerous vents collectively called Fossil Springs emanate from the Pennsylvanian Naco Limestone and coalesce to form Fossil Creek. In the early 1900s, diversion of spring water out of the natural channel began supplying 2 new hydroelectric power plants. Maximum power plant diversion capability is approximately equivalent to the nearly constant spring discharge. Consequently, with diversion of spring water, the potential for $CaCO_3$ precipitates that formed travertine structures in Fossil Creek was removed. Furthermore, runoff events from upper canyon reaches flowed over the diversion dams and through the natural channel eroding the existing travertine dams. Without the spring water to rebuild these travertine structures, only the erosional process remains.

Historic accounts of Fossil Creek prior to water diversion describe an extensive travertine system. In the late 1800s, the naturalist Charles Lummis (1891) reported that Fossil Springs water was so impregnated with minerals that "...it was constantly building great round basins for itself, and for a long distance flows over bowl after bowl". Lummis did not report the size or extent of

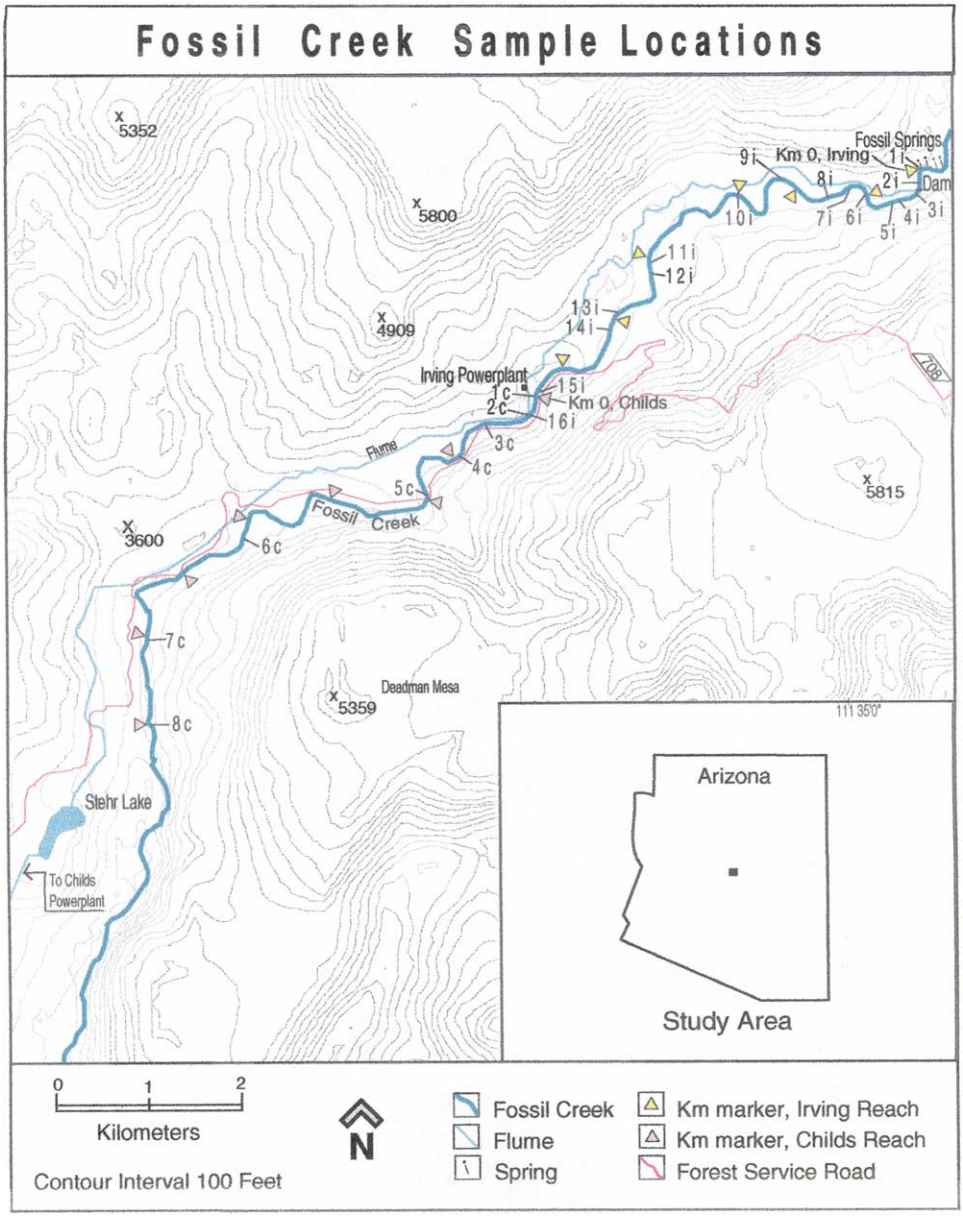

Fig. 1. Location map and site map showing topography, cultural features, and sample locations.

the travertine formations, but a later visitor, F.M. Chamberlain (1904) wrote "...the travertine structures persisted in a two mile reach of the creek. The largest pool seen was behind a ten foot tall travertine dam, 50 to 60 yards long, 20 to 30 feet wide, and approximately 20 feet or more deep". Overby and Neary's (1996) reconnaissance trip to map travertine structures in Fossil Creek located a minimum of 80 of these remnant dams below Fossil Springs.

In 1994, the Federal Energy Regulatory Commission (FERC) in cooperation with the US Forest Service began a review of Arizona Public Service (APS) license to continue diverting flow from Fossil Creek for power generation. The Federal Power Act requires hydroelectric power operators to be periodically reevaluated to reflect changing social values, operational advancements, or other factors (Federal Power Act, 1920). During reevaluation, this study was conducted to determine if the potential for travertine formation in Fossil Creek still existed, to quantify that potential if possible, determine the effect of proposed flow alternatives on stream morphology, and gain insight about the biological and overall precipitation dynamics of the system.

Quantification of CO_2 outgassing and $CaCO_3$ precipitation based on water chemistry and corresponding water volume was needed to determine the rate and location of travertine formation. Comparisons between calculated $CaCO_3$ mass transfer rates and precipitation rates on artificial substrates are addressed in this paper. The artificial substrate derived rates permitted observation of the role bed form morphology and flow patterns have on precipitation rates. An important component is the role of aquatic organisms and organic debris in the dynamics of calcite deposition in travertine depositing streams. The artificial substrates were used to quantify the role of organic material on travertine deposition rates. In addition, measurement of diurnal changes in conductivity, pH, and temperature were used to quantify the effects of photosynthetic activity on chemical changes in the water.

2. Site description

The study area is located along Fossil Creek, a tributary of the Verde River, which drains a portion of the Mogollon Rim in central Arizona (Fig. 1). Erosion of flat-lying sedimentary and volcanic strata of the region has left a mesa/canyon morphologic setting. Elevations within the watershed range from 2212 m at the Mogollon Rim to 777 m at the confluence with the Verde River. Plant communities vary from enclaves of Canadian species, including: *Pseudotsuga menziesii* (Poir.) Britton and *Populus tremuloides* (Michx.) on higher, protected slopes to upper Sonoran species at the Verde River confluence. The riparian plant community is dominated by *Platanus wrightii* (Wats.), *Alnus oblongifolia* (Torr.), and *Populus* spp.

The springs are located just below the edge of the Mogollon Rim at the southern margin of the Colorado Plateau in Fossil Creek Canyon, Arizona (Fig. 1). North of Fossil Springs steep-walled canyons cut into flat-lying Paleozoic sedimentary rocks, whereas south of the springs the canyon is composed of Tertiary volcanic rocks. Approximately 1000 m of Paleozoic and Cenozoic strata are exposed within the canyon. Paleozoic stratigraphy of the canyon includes the Mississippian Redwall Limestone, Pennsylvanian Naco Formation, Pennsylvanian/Permian Supai Formation, Permian Schnebly Hill Formation, Coconino Sandstone and Permian Kaibab Formation (Blakey, 1990). South of Fossil Springs, the volcanic rocks, chiefly dark-gray basalt and yellowish-gray tuff, thicken abruptly to more than 600 m along the ancestral Mogollon Rim (Twenter, 1962). A unique feature of the area is a prehistoric travertine deposit (Pleistocene and Holocene) that forms a conspicuous bench above Fossil Springs (Weir et al., 2002).

Fossil Springs consists of several vents along a 200 m reach of Fossil Creek, at or near channel level (Feth and Hem, 1962). It is the largest concentration of spring-water discharge in the Mogollon Rim region. Measurements taken from June 1946 to July 1952, resulted in 1172 l $s^{-1}$to 1210 l s^{-1} of spring-water discharge with a constant temperature between 21 and 22 °C (Feth and Hem, 1962). Analyses of gaging data from the Irving power station indicate water from the springs temporally dominated the flow with surface runoff contributions totaling less than 20% of the time prior to diversion (Loomis, 1994 unpublished Tonto National Forest technical report).

3. Materials and methods

Two discrete stream reaches were sampled above and below the upper powerplant at Irving (Fig. 1). The upper reach begins at the springs, site 1i (Fig. 1), continues past the upper diversion dam, site 2i (Fig. 1), which supplies water to the Irving powerplant. It ends just below a lower diversion dam, site 16i (Fig. 1), which is just upstream from the Irving powerplant. This reach is 6.7 km long with 16 sample locations. Sampling of this reach occurred on March 6, 1996, during 1218 l s^{-1}full baseflow that emanates solely from Fossil Springs. A second sampling occurred on December 5, 1996, during 5.6 l s^{-1} seepage flow. The 5.6 l s^{-1} flow is a result of seepage past the upper diversion dam, which is currently the normal flow volume for the reach between this dam and the Irving powerplant.

The lower reach begins at the Irving powerplant tailrace, where a portion of the water used to operate the turbines is discharged back into the stream channel

(Fig. 1). The lower reach is 7 km long with 8 sample locations, sites 1c–8c (Fig. 1). Sampling of the lower reach occurred on December 11, 1996, and again January 24, 1997, during a high snowmelt event. Discharge from the tailrace was 56.6 l s^{-1} during the first sample period. At each sampling location, conductivity, pH, temperature, and dissolved CO_2 (Orion Research, 1982) were measured on-site. The CO_2 probe measures the activity of dissolved CO_2 based on a 3-point calibration curve using $NaHCO_3$ standards with an acetic acid buffer. Three filtered samples (0.45 μm) were collected at each location, two in 80 ml acid-washed polyethylene bottles, and a third in a brown glass Teflon-septa bottle. An unfiltered sample was also collected for total cation analyses. The cation sample bottles were acidified with ultra-pure HNO_3 to a pH of less than 2 to prevent negative functional group sorption of the cations. The glass bottle samples were refrigerated and analyzed within 2 days of collection for dissolved inorganic C (DIC). Diurnal fluctuations in pH, conductivity, and temperatures at a single location in the lower reach were obtained using a HydroLab Datasonde 3 multi-parameter water quality instrument.

Dissolved inorganic C was measured using a Dohrmann Carbon Analyzer (Model DC-180) by non-dispersive infrared detection of UV radiated and persulfate oxidized dissolved organics (ASTM, 1988). This measurement includes all of the inorganic C, not just the dissolved CO_2 activity measured by the ISE probe described above. Ion analyses were performed using ion chromatography separation and conductivity detection (Dionex Corp., Sunnyvale, CA). The anion analyses used an AG4A-Sc (4×250 mm) column with 1.8 mM Na_2CO_3 eluent to determine F^-, Cl^-, NO_2^-, PO_4^-, Br^-, NO_3^-, and SO_4^{2-} (ASTM, 1992). Cation analyses used a CS12A (4×250 mm) column with 20 mM methanesulfonic acid eluent to determine Li^+, Na^+, NH_4^+, K^+, Mg^{2+}, and Ca^{2+} (Dionex, 1995).

Precipitation rates of $CaCO_3$ were calculated using mass transfer from solution and deposition on artificial substrates. Calcium carbonate mass transfer from solution to channel bed (mol l^{-1}) was determined by the change in Ca^{2+} between successive sampling points (Lorah and Herman, 1988). The molar quotient of Ca^{2+}/CO_3 is unity therefore mass transfer due to $CaCO_3$ precipitation can easily be calculated. Rate of $CaCO_3$ precipitation (mol l^{-1} s^{-1}) was determined by dividing each mass transfer by a reaction time. Reaction times were estimated using distance between sample points divided by average flow velocity. Average flow velocities and wetted surface area measurements were gathered during stream discharge measurements. Assuming a smooth rectangular shape, the wetted surface area of a reach was estimated by

$$A = 2ld + wl$$

where l is the length of the reach, d is the average depth, and w is the average width. Because a smooth channel was assumed, and channel roughness can add considerably to the wetted surface area, the calculated wetted surface area is a conservative estimate.

Carbon dioxide mass transfers were determined by the difference between molar concentrations of DIC removed from the system between successive sampling points, then corrected for loss of $CaCO_3$ by precipitation. A net loss of CO_2 implies outgassing. Mass transfers were normalized using approximate wetted surface area of a reach and the associated discharge to allow comparison between mass transfer data (mol l^{-1}) and $CaCO_3$ precipitation rates onto artificial substrates (mol cm^{-2} s^{-1}). Normalization was accomplished by dividing mass transfer by the product of discharge and wetted surface area.

Ion activities were calculated from ion concentrations, pH, and temperature data for each sample using WATEQ4F, an equilibrium speciation computer program for geochemical modeling (Plummer et al., 1976). WATEQ4F also calculates saturation indices of minerals, solution charge balances, and CO_2 partial pressures (P_{CO_2}) in equilibrium. A saturation index of $CaCO_3$ equals the logarithm of the ratio of ion activity product divided by equilibrium solubility product at sample temperature. A zero value indicates equilibrium, less than zero is undersaturated, and greater than zero is supersaturated. The charge balance equals the sum of anions minus cations divided by the sum of anions and cations, all in eq l^{-1} (Table 1). The charge balance is a quality control measure of the analyses, testing cation or anion deficiency. WATEQ4F was also used to compare temperature effects on conductivity and pH with HydroLab data.

WATEQ4F calculates CO_2 values as P_{CO_2} based on equilibriums using activities determined from solution chemistry. On-site field ion selective electrodes (ISE) measure activity of the gas phase in mg l^{-1}. For comparative purposes, conversion of ISE data (mg l^{-1}) to partial pressures was performed using the equation:

$$P_{CO_2} = a^*_{H_2CO_3}/K_{CO_2}$$

where K_{CO_2} is a temperature-dependent equilibrium constant obtained from Drever (1988). The H_2CO_3* term refers to dissolved aqueous CO_2 plus the concentration of undissociated H_2CO_3. Because the temperature of the waters sampled was near 25 °C, H_2CO_3* is almost completely comprised of the unhydrated species (Stumm and Morgan, 1981). Therefore, $a_{H_2CO_3}$* is within 99.8% of the a_{CO_2} obtained from the ISE measurement.

Artificial substrate data provides physical mass of $CaCO_3$ deposited on a surface area over time (mol cm^{-2} s^{-1}). The mass of $CaCO_3$ accumulated, divided by the product of substrate surface area and reaction time equals the precipitation rate (mol cm^{-2} s^{-1}). Calculated

substrate surface areas averaged 300 cm^2. At active dam sites, little to no $CaCO_3$ deposition occurred on the lower half of the substrate due to rapid cementing to the dam structure. Subsequently, a surface area equivalent to the upper portion of the substrate (150 cm^2) was used for these sites.

Physical estimates of the mass of $CaCO_3$ precipitation were measured by weighing deposits on the inert stainless steel screens. No surface conditioning of the screens was performed. The screens were weighed, followed by estimation of the surface area using a micrometer and simple geometry prior to installation. These screens were placed on active travertine dams below the Irving powerplant; sites 2c, 3c, and 5c (Fig. 1) where $CaCO_3$ deposition appeared to be preferentially concentrated. Where no dams were present, screens were placed in locations of similar flow patterns and substrate conditions as those at actively aggrading dam sites (sites 7c and 8c; Fig. 1).

Upon removal from stream locations, the screens were heated to 100 °C for 3 days to induce dehydration, weighed, then reheated to 500 °C for an hour to incinerate all the organic material, and weighed again. Decomposition of $CaCO_3$ does not occur below 800 °C (Greensberg et al., 1992). Using incremental heating and gravimetric methods allowed the mass of organic and mineral fractions to be calculated. If any clay minerals are incorporated in the sample, they are likely to possess bound water that is released between 150 and 300 °C possibly introducing a slight error in the calculation of the organic fraction.

4. Results and discussion

4.1. CO_2 outgassing

Both the ISE measured and WATEQ4F calculated P_{CO_2} levels emerging from the spring vents (site 1i) were approximately 150 times greater than normal atmospheric conditions (Table 2). This P_{CO_2} level is within those observed in soil zones by Atkinson and Smith (1976), therefore, regional thermal activity is not required as a source, but still could be a contributor to the elevated P_{CO_2}. The steep chemical gradient drives CO_2 outgassing during equilibration with the atmosphere (Jacobson and Langmuir, 1970; Langmuir, 1971). Initial rates of outgassing were high followed by

Table 1
Chemical analyses and charge balance for water sampled at Fossil Springs on 3/6/96

Temp. (°C)	pH	DIC	H_2CO_3	HCO_3^-	CO_3^{2-}	Cl^- (mg/l)	SO_4^{2-}	Ca^{2+}	Mg^{2+}	K^+	Na^+	Charge balance (%)
21.8	7.06	111.0	99.0	466.1	0.2	8.9	29.4	102.6	38.5	1.5	11.9	1.28

Table 2
CO_2 concentration data calculated by WATEQ4F and ISE for the upper reach

Sample site (km downstream)	WATEQ4F Log P_{CO_2}		ISE Log P_{CO_2}	
	Baseflow	Seepage	Baseflow	Seepage
1i (0.0)	−1.43	−1.31	−1.44	−1.31
2i (0.25)	−1.80	−1.65	−1.80	−1.44
3i (0.4)	−2.15	−2.45	−1.73	−1.63
4i (0.65)	−2.64	−2.64	−2.34	−1.77
5i (0.75)	−2.62	–[a]	−1.92	–[a]
6i (1.1)	−2.75	−2.30	−1.72	−1.69
7i (1.3)	−2.83	−2.68	−2.01	−1.54
8i (1.6)	−2.87	−2.87	−1.99	−1.39
9i (2.25)	−3.00	−2.71	−1.80	−1.63
10i (3.0)	−3.13	−2.24	−2.31	−1.60
11i (4.2)	−3.21	−2.75	−2.41	−1.43
12i (4.3)	−3.28	−2.92	−2.03	−1.75
13i (4.9)	−3.28	−2.89	−2.28	−1.62
14i (5.2)	−3.25	−3.00	−2.20	−1.78
15i (6.45)	−3.22	−2.70	−2.19	−1.64
16i (6.7)	−3.31	–[a]	−2.38	–[a]

[a] Not sampled due to inadequate water level at these sites.

rapid decreases in the outgassing rate with distance downstream. The rate of change in P_{CO_2} levels in the upper reach, from the springs to 650 m downstream, was approximately equal for both sampled flows (Table 2). From this point on downstream, seepage flow P_{CO_2} levels were higher and more variable than high flow levels (Table 2). The lowest P_{CO_2} levels occur approximately 4.3 km downstream, the location of the largest waterfall along the upper reach (site 12i) (Table 2). The lower P_{CO_2} levels measured at the higher flows and the minimum observed P_{CO_2} levels at each flow being located at the waterfall demonstrates the influence turbulence has on P_{CO_2} levels. The higher flows are more turbulent resulting in lower P_{CO_2} levels, while steep stream gradients at the waterfall also increases turbulence resulting in the lowest P_{CO_2} levels measured.

Water released at the Irving powerplant tailrace (site 1c) was approximately 20 times greater than normal atmospheric P_{CO_2} (Table 3). This initial concentration of P_{CO_2} is lower than levels at the springs, indicating significant outgassing between Fossil Springs and the tailrace. Outgassing occurred during transport in the flume and/or as it passes through the turbines at the Irving powerplant. Although ISE CO_2 concentrations were consistently higher than WATEQ4F concentrations, both techniques show rapid decreases in CO_2 within the first 400 m downstream from the Irving powerplant tailrace (Table 3).

Table 3
CO_2 concentration data calculated by WATEQ4F and ISE for the lower reach

Sample site (km downstream)	WATEQ4F Log P_{CO_2}		ISE Log P_{CO_2}	
	12/11/96	1/24/97	12/11/96	1/24/97
1c (0.0)	−2.23	−2.21	−1.16	−1.50
2c (0.1)	−2.68	−2.84	−1.35	−1.66
3c (0.4)	−2.70	−2.83	−1.62	−2.07
4c (0.8)	−2.76	−2.81	−1.45	−2.03
5c (1.8)	−2.91	−2.86	−1.92	−2.07
6c (4.2)	−3.02	−3.02	−1.95	−2.44
7c (6.1)	−3.11	−3.04	−1.62	−2.12
8c (7.0)	−2.94	−3.06	−1.43	−2.19

Table 4
Mass transfer and reaction rates for the upper reach

Sample site (km downstream)	Baseflow			Seepage flow		
	CO_2 (mol l^{-1} s^{-1})	$CaCO_3$ (mol l^{-1} s^{-1})	$CaCO_3$ (kg d^{-1})	CO_2 (mol l^{-1} s^{-1})	$CaCO_3$ (mol l^{-1} s^{-1})	$CaCO_3$ (kg d^{-1})
1i (0.0)						
2i (0.25)	−1.11E-06	6.73E-08		−6.04E-08	−9.13E-10	0
3i (0.4)	−4.33E-07	1.29E-08		−1.34E-07	−6.93E-08	7
4i (0.65)	1.87E-07	−1.46E-07	839	8.69E-09	−8.53E-08	14
5i (0.75)	−5.30E-07	3.38E-08	−78	–[a]	–[a]	
6i (1.1)	3.41E-08	−1.23E-07	995	2.86E-08	−2.33E-08	7
7i (1.3)	−4.48E-08	−1.51E-07	694	−2.54E-08	1.48E-09	0
8i (1.6)	−7.66E-08	−3.33E-08	230	−8.71E-11	−8.21E-09	2
9i (2.25)	4.66E-08	−1.58E-07	2374	2.20E-09	−7.91E-09	3
10i (3.0)	−3.28E-08	−9.03E-08	1560	−4.47E-10	4.69E-09	−2
11i (4.2)	2.93E-08	−7.21E-08	1993	4.85E-09	−6.97E-09	5
12i (4.3)	−3.76E-07	−1.02E-07	236	1.02E-08	−2.66E-08	2
13i (4.9)	−9.38E-08	−3.02E-08	417	−1.43E-08	−2.20E-08	8
14i (5.2)	1.75E-08	−9.51E-08	658	2.91E-09	−5.32E-09	1
15i (6.45)	5.46E-09	−2.24E-08	646	7.07E-09	−1.18E-09	1
16i (6.7)	1.75E-08	−2.41E-07	1388	–[a]	–[a]	
	Total		11,952			47

[a] Not sampled due to inadequate water level at these sites.

Table 5
Mass transfer and reaction rates for the lower reach

Sample site (km downstream)	12/11/96			1/24/97		
	CO_2 (mol l^{-1} s^{-1})	$CaCO_3$ (mol l^{-1} s^{-1})	$CaCO_3$ (kg d^{-1})	CO_2 (mol l^{-1} s^{-1})	$CaCO_3$ (mol l^{-1} s^{-1})	$CaCO_3$ (kg d^{-1})
1c (0.0)						
2c (0.1)	−3.36E-07	−3.91E-07	92	6.64E-08	−5.75E-07	
3c (0.4)	2.80E-08	−3.76E-08	27	−7.37E-08	1.09E-07	−77
4c (0.8)	−4.11E-08	−3.20E-08	30	−5.03E-08	−3.31E-09	3
5c (1.8)	5.17E-09	−4.74E-08	112	2.72E-08	−3.82E-08	90
6c (4.2)	2.79E-09	−2.76E-08	156	6.86E-09	−2.30E-08	130
7c (6.1)	7.30E-09	−1.72E-08	77	1.43E-09	−1.34E-08	60
8c (7.0)	−4.09E-10	−1.26E-08	27	3.69E-09	−1.22E-08	26
	Total		519			231

The discrepancy between ISE and WATEQ4F P_{CO_2} levels indicate a higher level of disequilibrium with the atmosphere than the equilibrium P_{CO_2} conditions derived using WATEQ4F. Though initial CO_2 concentrations for both sampled reaches are substantially different, P_{CO_2} values converge above equilibrium at approximately 1.5 km down their respective flow paths (Tables 2 and 3). The highest CO_2 mass transfer rate was measured at site 1c, just below the Irving powerplant tailrace (Table 5), even though steeper chemical gradients exist at site 1i at the springs (Table 4). Carbon dioxide flux across the air-water interface, as demonstrated by Usdowski and Hoefs (1990) static film model, is dependent on the transfer coefficient and concentration gradient between air and water. An exponential decline in dissolved CO_2 corresponding to the transfer coefficient occurs with time if turbulence and temperature are held constant. An increase in either turbulence or temperature increases the rate of decline in dissolved CO_2 with time. Hence, outgassing rates should be highest with steep chemical gradients and/or the greatest level of turbulence. Turbulence created high mass transfer rates in the lower reach from water passing through the power turbines immediately followed by a release over a small cascade below the tailrace (Table 5). The second highest CO_2 mass transfer rates were associated with the steep chemical gradient that occurs between the atmosphere and CO_2 supersaturated water emerging from the springs (Table 4).

Comparison of the two reaches illustrates the effect of CO_2 mass transfer rates at different P_{CO_2} on $CaCO_3$ mass transfer rates. Initial discharge at both reaches (1i, 1c) had the largest CO_2 mass transfer rates (Tables 4 and 5). In the upper reach, high CO_2 mass transfer rates did not correlate with high $CaCO_3$ mass transfer rates (Table 4) as they did along the lower reach (Table 5). This is because high initial P_{CO_2} (Table 2) did not decrease enough to surpass the kinetic barrier required for $CaCO_3$ precipitation.

Seepage flow P_{CO_2} (Table 2, WATEQ4F and ISE data) and pH (Table 6) showed substantial fluctuation compared with baseflow. Biochemical activity appears to be influencing P_{CO_2}. This can increase pH (photosynthetic activity) or lower pH (respiration). This trend was not distinguishable during baseflow. Baseflow, being 215 times greater than seepage flow, masks biochemical demand, which is approximately equal during both flows. Effects of biological activity on water chemistry were also observed along the lower reach. A Hydrolab Datasonde 3 recorded diurnal fluctuations of 0.40 pH units and 40 μS cm^{-1} at a location approximately 200 m below the tailrace. Effects of diurnal temperature fluctuations modeled using WATEQ4F revealed no pH change and a shift in conductivity of less than 2 μS cm^{-1}. These results suggest that the diurnal trends recorded by the data logger are a result of biochemical demand or production of CO_2.

Little information exists on the CO_2 outgassing rates from natural systems, however Pentecost's (1995) field study of Bagnaccio hot springs in Italy showed exponential decline in CO_2, which is consistent with the observations at Fosssil Springs and the static film model. Also, detailed investigations of travertine-depositing streams in Virginia indicate a positive relationship between mean shear stress of water in channels (turbulence) and CO_2 outgassing (Lorah and Herman, 1990). The level of CO_2 supersaturation and degree of turbulence is believed to influence the rate of CO_2 outgassing (Hubbard and Herman, 1990). Other mechanisms contributing to outgassing include consumption during $CaCO_3$ precipitation and biochemical activity (Dandurand et al., 1982; Pentecost, 1995). Additionally, decreases in pressure and increases in temperature will also cause CO_2 outgassing.

4.2. $CaCO_3$ precipitation

Chemical analyses of water samples taken along the upper sampled reach showed decreases in Ca^{2+} and HCO_3^- concentration as pH values increased (Table 6 and 7). Repeated analyses from the same spring vent (1i) for both sampling periods in the upper reach were approximately equivalent in ion concentration. Calcium and HCO_3^- concentrations of the water in the first 2 km decreased more during seepage-flow than baseflow (Tables 6 and 7). During both sampled flows at the lowermost site in the upper reach, Ca^{2+} concentration of the water was approximately equivalent, while HCO_3^- concentration was higher during seepage-flow (Tables 6 and 7). Trends in pH for the first 4 sample sites (1i–4i) were similar for both flow events. Downstream sites below 1i–4i had lower and more variable pH during seepage flow (Tables 6 and 7). This variability in low flow pH is associated with biochemical activity effecting CO_2 concentrations. In general, both Ca^{2+} and HCO_3^- concentrations decreased downstream, while other ion species remained relatively constant (Tables 6 and 7).

In the lower reach below the Irving powerplant, Ca^{2+} and HCO_3^- concentrations of the water also decreased with increased pH values (Tables 8 and 9). Return flow samples were very similar to the spring vents with respect to Ca^{2+} and HCO_3^- concentrations, suggesting little deposition of $CaCO_3$ occurs in the flume or at the

Table 6
Chemical data for upper reach for baseflow conditions

Sample site (km downstream)	Temp (°C)	pH	Cond. (μS cm^{-1})	DIC	H_2CO_3	HCO_3^- (mg l^{-1})	CO_3^{2-}	Ca^{2+}	$SI_{calcite}$
1i (0.0)	21.8	7.06	718	111.0	99.0	466.1	0.2	102.6	0.18
2i (0.25)	21.6	7.41	720	97.2	42.8	451.3	0.5	104.1	0.52
3i (0.4)	21.4	7.76	678	93.9	19.4	456.9	1.1	104.3	0.86
4i (0.65)	20.2	8.25	688	94.4	6.4	470.0	3.4	101.1	1.31
5i (0.75)	20.5	8.22	662	91.8	6.7	456.8	3.1	101.4	1.28
6i (1.1)	20.0	8.34	664	90.2	5.0	449.2	4.0	97.6	1.37
7i (1.3)	19.6	8.40	696	88.1	4.3	439.0	4.5	94.9	1.40
8i (1.6)	19.6	8.43	689	86.4	3.9	430.3	4.7	94.1	1.41
9i (2.25)	19.8	8.47	642	82.6	3.4	411.2	5.0	85.0	1.40
10i (3.0)	19.8	8.52	608	77.7	2.8	386.8	5.3	79.1	1.39
11i (4.2)	20.4	8.63	604	75.0	2.1	372.5	6.5	71.5	1.44
12i (4.3)	20.7	8.70	583	72.5	1.7	359.2	7.4	70.6	1.49
13i (4.9)	20.4	8.74	515	68.6	1.5	339.3	7.6	69.0	1.49
14i (5.2)	20.2	8.70	579	67.4	1.6	333.8	6.9	66.5	1.43
15i (6.45)	20.0	8.67	535	66.3	1.7	328.6	6.3	64.1	1.38
16i (6.7)	18.7	8.73	522	63.3	1.4	313.4	6.9	58.8	1.37

Table 7
Chemical data for upper reach during seepage flow conditions

Sample site (km downstream)	Temp (°C)	pH	Cond. (μS cm^{-1})	DIC	H_2CO_3	HCO_3^- (mg l^{-1})	CO_3^{2-}	Ca^{2+}	$SI_{calcite}$
1i (0.0)	21.5	6.90	747	106.3	127.3	414.6	0.1	100.5	−0.03
2i (0.25)	21.0	7.27	747	101.5	59.8	456.3	0.3	100.4	0.36
3i (0.4)	16.4	8.03	723	91.9	10.3	454.5	2.0	94.9	1.02
4i (0.65)	8.2	8.15	686	85.8	7.4	426.3	2.5	83.7	0.94
6i (1.1)	11.1	7.82	675	86.6	15.6	423.3	1.1	78.2	0.63
7i (1.3)	9.4	8.19	669	85.1	6.7	422.9	2.7	78.3	0.97
8i (1.6)	6.1	8.37	655	84.3	4.4	419.8	4.0	77.0	1.08
9i (2.25)	7.6	8.21	655	83.1	6.2	413.3	2.7	74.3	0.93
10i (3.0)	12.3	7.76	658	84.1	17.3	409.3	1.0	76.2	0.57
11i (4.2)	9.1	8.25	666	83.3	5.7	414.6	3.0	71.8	0.98
12i (4.3)	8.1	8.42	661	82.8	3.8	412.4	4.4	70.4	1.11
13i (4.9)	8.8	8.35	607	75.9	4.1	378.2	3.5	63.4	0.99
14i (5.2)	8.4	8.46	607	75.7	3.2	376.9	4.5	62.6	1.08
15i (6.45)	8.6	8.18	618	78.0	6.2	387.8	2.4	61.8	0.82

powerplant (Tables 6 and 8). The greatest change occurred at the first sampling interval between sites 1c and 2c for both sampling periods (Tables 8 and 9).

Calcite saturation indices from the spring vent (1i) were close to equilibrium upon emergence (Tables 6 and 7). Approximately 10 times $CaCO_3$ supersaturation of the water occurred at 400 m downstream, the result of CO_2 outgassing. Below 400 m, $CaCO_3$ saturation indices of the water for seepage flow were consistently lower and more variable than at baseflow (Tables 6 and 7). Both baseflow and seepage flow reached their greatest $CaCO_3$ saturation level just below the largest falls (12i), approximately 4300 m downstream from the springs (Tables 6 and 7). In the pool below the falls, $CaCO_3$ supersaturation levels of the water reached 31 times saturation during baseflow, while seepage flow levels were 13 times supersaturation.

Calcite saturation indices of the water from the lower reach were 5–7.5 times supersaturated (Table 8) at site 1c, located just below the Irving powerplant tailrace. The December 11, 1996 water samples reached a maximum of 17 times $CaCO_3$ supersaturation within 2 km downstream, while snow-melt diluted water samples reached an equivalent maximum 400 m downstream (Tables 8 and 9). The variation in saturation indices between the high and low flow in the upper reach, and intermediate lower reach flows demonstrate that higher flows reach a higher level of supersaturation as a result of increased CO_2 outgassing from the increased turbulence. At the furthest downstream site in the lower reach (8c), $CaCO_3$ saturation indices of the water for both sampling periods were approximately 10 times supersaturation (Tables 8 and 9).

As $CaCO_3$ saturation indices rise, the kinetic barrier to nucleation is exceeded and precipitation of $CaCO_3$ occurs (Barnes, 1965; Shuster and White, 1971; Jacobson and Usdowski, 1975). Field investigations of travertine-depositing streams show a 5 (Jacobson and Usdowski, 1975) to 10 times (Dandurand et al., 1982) level of $CaCO_3$ supersaturation is needed before precipitation will occur. Suarez (1983) did not detect $CaCO_3$ precipitation in the Colorado River with a 4.6 times supersaturation level.

Upper reach $CaCO_3$ mass transfer rates during baseflows began to increase approximately 500 m downstream of the sampled spring vent (1i) in association with the highest CO_2 outgassing rates (Table 4). Precipitation of $CaCO_3$ occurred roughly 500 m downstream where CO_2 outgassing rates exceeded and remained at -1×10^{-7} mol l^{-1} s^{-1}, with only one slightly positive calculated $CaCO_3$ mass transfer (Table 4). Overall, baseflow conditions had higher $CaCO_3$ mass transfer rates than seepage flows. Increased CO_2 outgassing correlates well with initial large increases in

Table 8
Chemical data for lower reach during 12/11/96

Sample site (km downstream)	Temp (°C)	pH	Cond. (μS cm^{-1})	DIC	H_2CO_3	HCO_3^- (mg l^{-1})	CO_3^{2-}	Ca^{2+}	$SI_{calcite}$
1c (0.0)	20.7	7.83	740	90.1	15.9	440.7	1.2	100.2	0.89
2c (0.1)	20.1	8.24	700	82.4	5.8	410.1	2.9	89.7	1.21
3c (0.4)	19.8	8.25	681	82.1	5.6	408.7	3.0	87.8	1.20
4c (0.8)	19.7	8.29	670	79.1	4.9	393.6	3.1	85.5	1.22
5c (1.8)	18.1	8.41	650	74.6	3.5	371.6	3.9	77.2	1.24
6c (4.2)	15.9	8.47	NA	68.4	2.8	340.4	4.1	65.6	1.17
7c (6.1)	14.7	8.54	NA	66.4	2.3	330.2	4.7	59.9	1.17
8c (7.0)	14.9	8.37	NA	65.2	3.4	324.6	3.1	57.9	1.00

Table 9
Chemical data for lower reach during 1/24/97

Sample site (km downstream)	Temp (°C)	pH	Cond. (μS cm^{-1})	DIC	H_2CO_3	HCO_3^- (mg l^{-1})	CO_3^{2-}	Ca^{2+}	$SI_{calcite}$
1c (0.0)	18.4	7.75	672	81.9	17.3	398.1	0.9	88.0	0.70
2c (0.1)	14.9	8.33	627	76.6	4.3	381.2	3.3	78.0	1.14
3c (0.4)	17.9	8.34	653	77.7	4.3	386.9	3.5	83.7	1.23
4c (0.8)	18.3	8.31	647	75.4	4.5	375.6	3.1	83.5	1.19
5c (1.8)	16.7	8.35	625	74.3	4.0	369.9	3.4	76.8	1.17
6c (4.2)	13.8	8.47	595	70.2	2.9	349.5	4.2	67.1	1.16
7c (6.1)	11.5	8.47	582	67.8	2.8	337.6	4.1	62.7	1.09
8c (7.0)	10.5	8.48	575	67.0	2.7	333.6	4.1	60.7	1.07

$CaCO_3$ saturation indices of the water, however this trend does not continue beyond the first 500 m (Tables 4, 6, and 7).

Seepage flow $CaCO_3$ mass transfers were near zero in slack water behind the upper diversion dam, then increased immediately below the dam (2i) and persisted downstream for approximately 1 km (6i) (Table 4). After 1 km, a general decrease in $CaCO_3$ mass transfer rates occurred for the remainder of the reach (Table 4). Higher $CaCO_3$ mass transfer rates did follow a trend during seepage flow with increased saturation indices (Table 7) and decreased WATEQ4F P_{CO_2} (Tables 2 and 4).

Calcite precipitation rates for each sample interval were also calculated in kg d^{-1} (Tables 4 and 5). Total $CaCO_3$ precipitation for the upper reach was calculated to be 11,952 kg d^{-1} for baseflow, and 47 kg d^{-1} for seepage-flow (Table 4). For the entire upper reach, the rate of $CaCO_3$ removed during both flows was equivalent. Equivalent rates will produce amounts of $CaCO_3$ deposition directly proportional to discharge. However, because baseflow conditions had lower CO_2 activities at the end of the sampled reach relative to seepage flow, it is likely that additional $CaCO_3$ mass transfer will occur below this site during baseflow conditions if water is not diverted out of the natural channel.

4.3. Comparisons of $CaCO_3$ precipitation methods and precipitation dynamics

Mass transfer of Ca^{2+} between successive sampling points was used to quantify precipitation using the same methods as Lorah and Herman (1988). Calcite transfer rates in the first 100 m of the lower reach were higher than any other downstream rates (Table 5). Changes in concentration caused by tailrace water mixing with seepage flow water in the main channel (between sample sites 1c and 2c—the first 100 m) were accounted for using simple volume and concentration relationships. The high mass transfer rates measured between 1c and 2c correlated with the highest CO_2 mass transfer rate (Table 5), low WATEQ4F P_{CO_2} (Table 3), and high $CaCO_3$ saturation indices (Tables 5 and 6). For the December 11, 1996 sampling, precipitation rates calculated for the entire lower reach resulted in 519 kg d^{-1} $CaCO_3$ deposition (Table 5).

Artificial substrate (screens) deposition rates were compared to $CaCO_3$ mass transfer rates calculated from chemical data obtained at the screen locations along the lower reach. Calcite mass transfer rates were normalized for wetted surface area within the interval bounded by sample locations. Calcite mass transfer rates are an average of the entire wetted surface area while screen rates represent site-specific deposition.

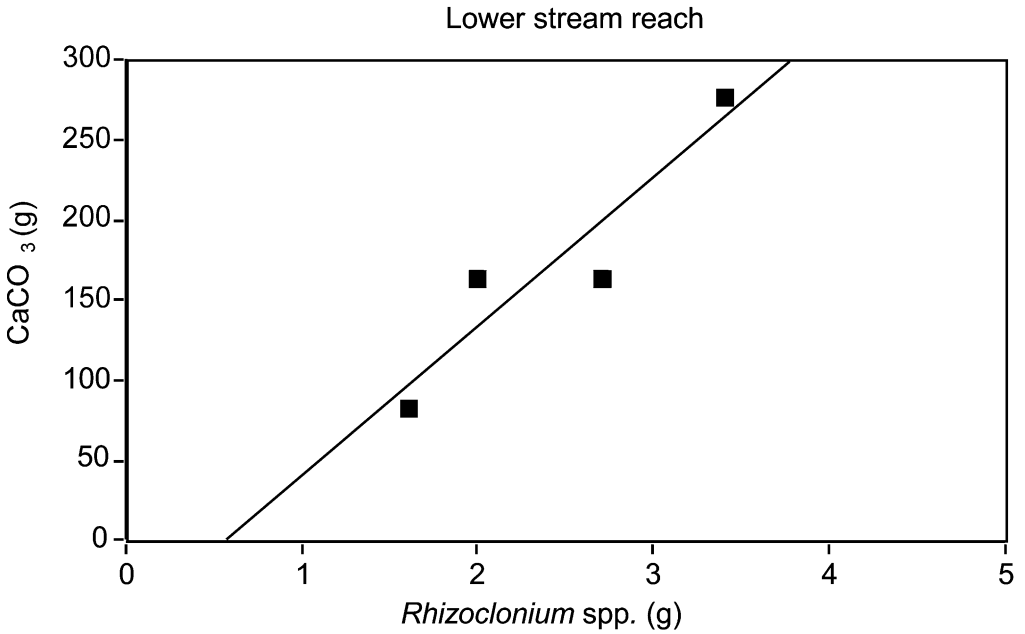

Fig. 2. Mass of algae versus $CaCO_3$ accumulated on artificial substrates in 44 days at Fossil Creek, Arizona. Individual boxes are averages of replicate analysis of single screens.

Visually the greatest precipitation appears to be on crests of active travertine dams. The screens were placed on the crests of dams to ensure deposition would occur. Liu et al. (1995) demonstrated that inorganic calcite precipitation occurs at a greater rate onto pure marble substrates under fast flow conditions created by the steep stream gradients at dam locations when compared to pools with identical hydrochemistry. If screen $CaCO_3$ deposition rates are greater than the calculated $CaCO_3$ mass transfer rates for the interval the screens are located in, then dam locations create an environment that is preferential for $CaCO_3$ precipitation. Calcite deposition rates obtained at screen site 2c, 100 m below the tailrace, were approximately equal to calculated $CaCO_3$ mass transfer rates, indicating preferential precipitation was not occurring at this site. Large dams and carbonate mud deposition on pool bottoms characterize this reach.

Screen rates at sample locations 3c and 5c were 6 and 9 times greater than $CaCO_3$ mass transfer rates indicating preferential precipitation. Small dams characterize this reach with little carbonate mud accumulation on the pool bottoms. No active dam formation was occurring at sites 7c and 8c, even though screens were located in areas with similar morphology to the upstream sites with dams. Screen $CaCO_3$ deposition rates obtained at these locations were approximately equal to $CaCO_3$ mass transfer rates.

Substrates located at actively forming dam locations (2c, 3c, 5c) also had greater amounts of organic material than those located at non-actively forming dam locations (7c, 8c). The accumulated porous travertine material contained abundant macro invertebrates with both living algal material and detrital organic debris included. At non-active dam locations only detrital organic debris accumulated.

Artificial substrate data (Fig. 2) indicate a correlation between mass of calcite deposited and mass of organic material. The filamentous green algae (*Rhizoclonium* spp.) are clearly associated with preferential $CaCO_3$ precipitation. Reasons for this may include one or more of the following: (1) large reactive surface area of the algal mat compared to other channel surfaces, (2) mucous excretions from bacteria and diatoms on the algae trap micritic particles that behave as seed crystals, and (3) photosynthetic uptake of CO_2 by algae raises pH enough to allow precipitation to occur (Emeis et al., 1987).

It is not known which factor or combination of factors facilitate preferential deposition on organic substrates, but algal mats along Fossil Creek appear to play a major role. As precipitation proceeded, filamentous green algae (*Rhizoclonium* spp.) became encrusted, yet still remained porous and permeable. These porous algae-laden dams are ideal for further deposition as increasing surface area during algal growth is continuously bathed in supersaturated $CaCO_3$ water. Observations made by Emeis et al. (1987) when studying the travertine system at Plitvice National Park in Croatia support the importance of biological activity in travertine deposition. Emeis et al. (1987) used two different substrates, stainless steel and Cu (an algaecide), to compare precipitation rates. The stainless steel sponges showed abundant algal growth and calcite deposition, while Cu sponges had accumulations of neither. Contrary to the findings at Fossil Creek and Plitvice National Park, a study at Huanglong Gorge by Lu et al. (2000) found that microorganisms may actually aid dissolution of calcite and that algal photosynthesis is unimportant in $CaCO_3$ deposition. Additionally, a study of Le Zitelle Springs in Italy by Folk (1994) had intermediary results showing that precipitation occurred on Cu substrates, but at a greatly reduced rate as compared to organic substrates. Because of the varying effects of biological activity observed on travertine deposition at the various locations, it becomes obvious that a continuum of travertine degrading and aggrading processes can result from biological activity depending on site-specific conditions.

5. Conclusions

Carbon dioxide outgassing and $CaCO_3$ precipitation are the controlling processes of the geochemical evolution of Fossil Springs' water. Precipitation of $CaCO_3$ was 11,952 kg d^{-1} at baseflow compared to 47 kg d^{-1} at seepage flow in the upper reach. In general, the potential for $CaCO_3$ deposition is directly proportional to flows; however, mass transfers of CO_2 and $CaCO_3$ are greater, and continue further downstream during the higher baseflows when compared to seepage flows. This phenomenon is attributed to the higher velocities and greater turbulence associated with baseflow.

Comparisons of mass transfer rates and rates obtained from artificial substrates in the lower reach demonstrate $CaCO_3$ precipitation is preferential to dam structures. Increased turbulence at dam crests is one possible mechanism, but the authors suspect that preferential deposition is also controlled by filamentous green algae acting as a nucleation surface for $CaCO_3$ deposition. Diurnal fluctuations in solution observed at 56.6 l s^{-1} flows imply a cyclic depositional trend dependent on biochemical activity. This affect is greater at low flow regimes and low P_{CO_2}. Declining P_{CO_2} facilitates $CaCO_3$ supersaturation, while channel localities with abundant reactive surface area and high water velocity facilitate precipitation.

This research demonstrates that geochemical processes that have the ability to restore the degraded travertine system in Fossil Creek do exist. Historical accounts and geochemical analyses indicate the majority of travertine deposition would occur along a 6.7 km

reach beginning at Fossil Springs. Calcite deposition would occur at a rate proportional to the amount of spring discharge allowed to flow down the natural channel. This sequence of long aggrading periods followed by short destructive flood events produces an active morphology in the Fossil Creek channel. Restoration of travertine dynamics from resumption of natural flows would create a rare natural phenomenon and an opportunity to further study processes of travertine formation.

Acknowledgements

Special thanks are due to Liz Matthews for her inspiration and technical expertise in fostering this research. We are also grateful to the Beaver Creek/Sedona Ranger District of the Coconino National Forest and Arizona Public Service for their cooperation during sampling. The Rocky Mountain Research Station in Flagstaff, Arizona provided financial support and laboratory facilities.

References

ASTM (American Society for Testing Materials), 1992. Standard Test Method For Anions in Water By Chemically Suppressed Ion Chromatography (D 4327). Am. Soc. Test. Matter, Philadelphia, PA.

ASTM (American Society for Testing Materials), 1988. Standard test method for total organic carbon in ground water monitoring (D 4779). Am. Soc. Test. Matter, Philadelphia, PA.

Atkinson, T.C., Smith, D.I., 1976. The erosion of limestones. In: Ford, T.D. (Ed.), The Science of Speleology. Academic Press, London, UK, pp. 151–178.

Barnes, I., 1965. Geochemistry of Birch Creek, Inyo County California: a travertine depositing creek in an arid climate. Geochimic. Cosmochim. Acta 29, 85–112.

Barnes, I., Irwin, W.P., White, D.E., 1984. Map showing world distribution of carbon dioxide springs and major zones of seismicity. US Dept. Int. Geol. Surv., Misc. Invest. Ser. Map I-1528.

Blakey, R.C., 1990. Stratigraphy and geologic history of Pennsylvanian and Permian rocks, Mogollon Rim region, central Arizona and vicinity. Geol. Soc. Am. Bull. 102, 1189–1217.

Cathelineau, M., Dubessy, J., Marignac, C., Valori, A., Gianelli, G., Puxeddu, M., 1989. Pressure-temperature-fluid composition changes from magmatic to present day stage in the Larderello geothermal field. In: Miles, D.L. (Ed.), Water-Rock Interaction. Balkema, Rotterdam, pp. 137–140.

Chamberlain, F.M., 1904. Notes on Work in Arizona—1904. Unpublished report on file with the Smithsonian Institution Archives, Washington, DC.

Dandurand, J.L., Gout, R., Hoefs, J., Menschel, G., Schott, J., Usdowski, E., 1982. Kinetically controlled variation of major components and carbon and oxygen isotopes in a calcite-precipitating spring. Chem. Geol. 36, 299–315.

Deines, P., 1992. Mantle carbon: concentration, mode of occurrence and isotopic composition. In: Schidlowski, M., Golubic, S., Kimberley, M.M., McKirdy, D.M., Trudinger, P.A. (Eds.), Early Organic Evolution. Springer, Berlin, pp. 133–146.

Dionex, 1995. Isocratic Elution of Six Cations. Dionex Corp, Sunnyvale, CA.

Drever, J.I., 1998. The Geochemistry of Natural Waters. Prentice Hall, Englewood Cliffs, NJ.

Emeis, K.C., Richnow, H.H., Kempe, S., 1987. Travertine formation in Plitvice National Park, Yugoslavia: chemical versus biological control. Sedimentol. 34, 595–609.

Federal Power Act, 1920. 16 USC 791-828C: Chapter 285, June 10, 1920; 4I STHE. 1063.

Feth, J.H., Hem, J.D., 1962. Springs along the Mogollon Rim in Arizona. In: Guidebook of the Mogollon Rim region, east-central Arizona. New Mexico Geol. Soc., 13th Field Conf., Socorro, N. Mex., pp. 129–134.

Folk, R.L., 1994. Interaction between bacteria, nonnobacteria, and mineral precipitation in hot springs of Central Italy. Geographie Physique et Quaternaire 48, 233–246.

Friedman, I., 1970. Some investigation of the deposition of travertine from hot springs—the isotopic chemistry of a travertine-epositing springa. Geochimic. Cosmochim. Acta 34, 1303–1315.

Greensberg, E.A., Clesceri, L.S., Eaton, A.D. (Eds.), 1992. Standard methods for the examination of water and wastewatereighteenth ed.. APHA-AWWA-WPCF, Washington, DC.

Hubbard, D.A., Herman, J.S., 1990. Overview of travertine_-marl volume. Travertine-marl: stream deposits in Virginia. Virginia Div. Min. Resour. 101, 1–4.

Hurley, P.M., Fairburn, H.W., Pinson Jr., W.H., 1966. Rb-Sr isotopic evidence in origin of potash-rich lavas of western Italy. Earth Planet. Sci. Lett. 5, 301–303.

Jacobson, R.L., Usdowski, E., 1975. Geochemical controls on a calcite precipitating spring. Contrib. Mineral. Petrol. 51, 65–74.

Jacobson, R.L., Langmuir, D., 1970. The chemical history of some spring waters in carbonate rocks. Ground Water 8 (3), 5–9.

Langmuir, D., 1971. The geochemistry of some carbonate groundwater in central Pennsylvania. Geochim. Cosmochim. Acta 35, 1023–1045.

Liu, Z., Svensson, U., Dreybrodt, W., Yuan, D., Buhmann, D., 1995. Hydrodynamic control of inorganic calcite precipitation in Huanglong Ravine, China: Field measurements and theoretical prediction of deposition rates. Geochim. Cosmochim. Acta 59, 3087–3097.

Lorah, M.M., Herman, J.S., 1988. Calcite precipitation rates in the field: measurement and prediction for a travertine depositing stream. Geochim. Cosmochim. Acta 52, 2347–2355.

Lorah, M.M., Herman, J.S., 1990. Geochemical evolution and calcite precipitation rates in falling spring creek, Virginia: Travertine-Marl: stream deposits in Virginia. Virginia Div. Min. Resour. Publ. 101, 17–32.

Lu, G., Zheng, C., Donahoe, R.J., Berry Lyons, W., 2000. Controlling processes in a $CaCO_3$ precipitating stream in Huanglong Natural Scenic District, Sichuan. China. J. Hydrol. 230, 34–54.

Lummis, C.F., 1891. The Greatest Natural Bridge on Earth. In Some Strange Corners of Our Country: The Wonderland of the Southwest. The Cadury Company, New York. pp. 142–145.

Orion Research, 1982. Model 95-02 Carbon Dioxide Electrode Instruction Manual. Orion Res, Cambridge, MA.

Overby, S.T., Neary, D.G., 1996. Travertine geomorphology of Fossil Creek. In: Proc. 1996 Meetings of the Arizona Section-American Water Resources Association, and the Hydrology Section, Arizona-Nevada Acad. Science, Vol. 16, Tucson, AZ 20 April 1996, pp. 9–12.

Pentecost, A., 1995. Geochemistry of carbon dioxide in six travertine-depositing water of Italy. J. Hydrol. 167, 263–278.

Plummer, L.N., Jones, B.F., Truesdell, A.H., 1976. WATEQ4F—A FORTRAN IV Version of WATEQ, a Computer Program for Calculating Chemical Equilibria of Natural Waters. U. S. Geol. Surv., Water Resour. Invest. 76–13.

Shuster, E.T., White, W.B., 1971. Seasonal fluctuations in the chemistry of limestone springs: a possible means for characterizing carbonate aquifers. J. Hydrol. 14, 93–128.

Stumm, W., Morgan, J.J., 1981. Aquatic chemistry. John Wiley & Sons, New York.

Suarez, D.L., 1983. Calcite supersaturation and precipitation kinetics in the lower Colorado River, All-American Canal and East Highland Canal. Water Resour. Res. 19, 653–661.

Twenter, F.R., 1962. The significance of the volcanic rocks in the Fossil Creek area, Arizona. In: Guidebook of the Mogollon Rim Region, East-central Arizona, New Mexico Geol. Soc., 13th Field Conf., Socorro, N. Mex., pp. 107–108.

Usdowski, E., Hoefs, J., 1990. Kinetic C^{13}/C^{12} and O^{18}/O^{16} effects upon dissolution and outgassing of CO_2 in the system CO_2-H_2O. Chem. Geol. 80, 109–118.

Weir, G.W., Beard, L.S. and Ellis, C.E. Mineral Resource Potential of the Fossil Springs Roadless Area, Yavapai, Gila and Coconino Counties, Arizona USGeol. Surv., in press.